13-4-2006

The fragmentation pathways of protonated Amiton in the gas phase: towards the structural characterisation of organophosphorus chemical warfare agents by electrospray ionisation tandem mass spectrometry

S. Ellis-Steinborner
Defence Science and Technology Organisation, Victoria

A. Ramachandran
University of Wollongong

Stephen J. Blanksby
University of Wollongong, blanksby@uow.edu.au

The fragmentation pathways of protonated Amiton in the gas phase: towards the structural characterisation of organophosphorus chemical warfare agents by electrospray ionisation tandem mass spectrometry

Abstract

Amiton (O,O-diethyl-S-[2-(diethylamino)ethyl] phosphorothiolate), otherwise known as VG, is listed in Schedule 2 of the Chemical Weapons Convention (CWC) and has a structure closely related to VX (O-ethyl-S-(2-diisopropylamino)ethyl methylphosphonothiolate). Fragmentation of protonated VG in the gas phase was performed using an electrospray ionisation ion trap mass spectrometer (ESI-ITMS) and revealed several characteristic product ions. Quantum chemical calculations provide the most probable structures for these ions as well as the likely unimolecular mechanisms by which they are formed. The decomposition pathways predicted by computation are consistent with deuterium labeling studies. The combination of experimental and theoretical data suggests that the fragmentation pathways of VG and analogous organophosphorus nerve agents, such as VX and Russian VX, are predictable and as such ESI tandem mass spectrometry is a powerful tool for the verification of unknown compounds listed in the CWC.

Disciplines

Life Sciences | Physical Sciences and Mathematics | Social and Behavioral Sciences

Publication Details

This article was originally published as: Ellis-Steinborner, S, Ramachandran, A & Blanksby, SJ, The fragmentation pathways of protonated Amiton in the gas phase: towards the structural characterisation of organophosphorus chemical warfare agents by electrospray ionisation tandem mass spectrometry, Rapid Communications in Mass Spectrometry, 2006, 20 (12), 1939-1948.

The fragmentation pathways of protonated Amiton in the gas phase: towards the structural characterization of organophosphorus chemical warfare agents by ESI-MS/MS

Simon Ellis-Steinborner[1*], Aravind Ramachandran[2], Stephen J. Blanksby[2*]

[1]Human Protection and Performance Division, Defence Science and Technology Organisation, 506 Lorimer Street, Fishermans Bend, Victoria, 3207, Australia.
[2]Department of Chemistry, University of Wollongong, Wollongong NSW, 2522, Australia.

Running Title: Fragmentation Pathways of Amiton in the Gas Phase

* *Correspondence to* S. Ellis-Steinborner, Human Protection and Performance Division, Defence Science and Technology Organisation, 506 Lorimer Street, Fishermans Bend, Victoria, 3207, Australia. Telephone: +61 8 8259 6007, Fax: +61 3 8259 6585, Email: simon.ellis-steinborner@dsto.defence.gov.au
S.J. Blanksby, Department of Chemistry, University of Wollongong, Wollongong, New South Wales, 2522, Australia, Telephone: +61 2 4221 5484, Fax: +61 2 4221 4287, Email: blanksby@uow.edu.au

ABSTRACT

Amiton (*O,O*-diethyl-*S*-[2-(diethylamino)ethyl] phosphorothiolate), otherwise known as VG, is listed in Schedule 2 of the Chemical Weapons Convention (CWC) and has a structure closely related to VX (*O*-ethyl-*S*-(2-diisopropylamino)ethyl methylphosphonothiolate). Fragmentation of protonated VG in the gas phase was performed using an electrospray ionisation ion trap mass spectrometer (ESI-ITMS) and revealed several characteristic product ions. Quantum chemical calculations provide the most probable structures for these ions as well as the likely unimolecular mechanisms by which they are formed. The decomposition pathways predicted by computation are consistent with deuterium labeling studies. The combination of experimental and theoretical data suggests that the fragmentation pathways of VG and analogous organophosphorus nerve agents, such as VX and Russian VX, are predictable and as such ESI tandem mass spectrometry is a powerful tool for the verification of unknown compounds listed in the CWC.

INTRODUCTION

Amiton (*O,O*-diethyl-*S*-[2-(diethylamino)ethyl] phosphorothiolate), otherwise known as VG, is listed in Schedule 2 of the Chemical Weapons Convention (CWC) and has a structure closely related to VX (*O*-ethyl-*S*-(2-diisopropylamino)ethyl methylphosphonothiolate) (see Figure 1).[1] VG was developed in the 1950's as a potential insecticide but after a limited distribution was found to be far too toxic for domestic use and therefore was not produced commercially.[2] VG has a similar toxicity to tabun and equivalent physical properties to VX and as such there is interest in its production and stockpiling among chemical warfare proliferators.[1,3] Several previous studies directed toward the detection of VG in various environmental matrices have used predominantly gas chromatography/mass spectrometry (GC/MS). While the characterization of VG degradation products has utilized a broad range of techniques including; mass spectrometry,[4] ^{31}P nuclear magnetic resonance (NMR),[5] ion-selective electrodes,[6] colormetric and fluorescence assays.[7,8]

Figure 1

In general, liquid chromatography/mass spectrometry (LC/MS) techniques are now routine in the analysis and identification of chemical warfare agents (CWAs), and related compounds, in the verification of the CWC. Several LC/MS techniques have been published for the analysis and identification CWA related compounds. These include the detection of CWA agents, precursors and degradation products within various matrices using both electrospray ionisation (ESI)[9-12] and atmospheric pressure chemical ionisation (APCI).[13-16] More than simply detection however, when dealing with the analysis of CWAs, it is critical to rapidly identify structural variations of

existing, well-characterized agents. For example, it is necessary to distinguish between VX and VG, which are structurally related (Figure 1). Previous studies have highlighted the utility of collision induced dissociation (CID) for the differentiation of structurally related CWAs. For example, analysis of VX and Russian VX (RVX, *O*-isobutyl-S-(2-diethylamino)ethyl methylphosphonothiolate) (see Figure 1) have been performed via direct flow injection analysis[17] and secondary ion mass spectrometry (SIMS) from concrete.[18,19] CID of the $[VX+H]^+$ and $[RVX +H]^+$ precursor ions revealed significant difference in the major fragment ions observed, consistent with the structure of organophosphates. A general decomposition pathway to account for the observed fragments is outlined in Scheme 1.

Scheme 1.

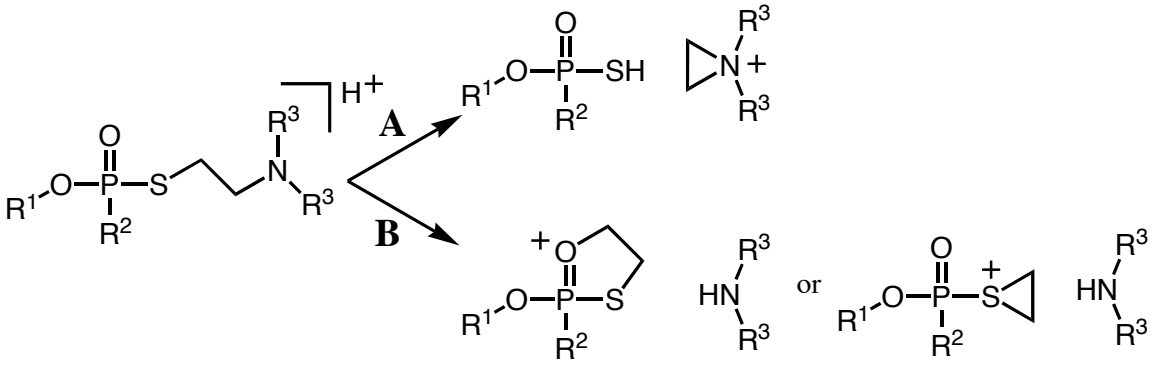

Abundant fragment ions corresponding to disubstituted aziridines are formed from CID of both protonated VX and RVX and are observed at *m/z* 128 (*N,N*-diisopropyl aziridine) and *m/z* 100 (*N,N*-diethyl aziridine), respectively (Scheme 1A). Less abundant fragments are observed at *m/z* 167 and *m/z* 195 for VX and RVX, respectively and correspond to neutral loss of the dialkyl amine in each case (Scheme 1B). Therefore, the two fragmentation pathways outlined in Scheme 1 suggest that ESI-MS/MS provides a simple method for differentiating VX and RVX and perhaps

for the structural characterization of other related CWAs. To this point, no tandem mass spectrometric studies of structurally related VG have been found in the open literature and furthermore, the structure of the ions formed during the extrusion of the neutral amine (Scheme 1B) have not been unambiguously determined.

In the present study we characterize the fragmentation of protonated VG using positive ion ESI tandem mass spectrometry in a quadrupole ion trap instrument and compare its fragmentation behaviour to both VX and RVX. Furthermore, we present hybrid density functional calculations that compare the relative stability of product ions formed in the fragmentation pathways and additionally calculate and compare the activation barriers of the major fragmentation pathways to confirm the product ion structures. These data provide an understanding of the mechanisms by which organophosphorus CWA fragments in an effort to assist the identification of unknown agents for verification of the CWC.

METHODS

Mass Spectrometry

VG was synthesized in-house to a purity of greater that 95% (*N.B.* the synthetic method is not provided in this manuscript for security reasons). The estimated purity was determined by ^{1}H and ^{31}P NMR, GC/MS and LC/MS. Acetonitrile (HPLC Grade, EM Scientific) was obtained from Crown Scientific (Sydney NSW, Australia). Deuterium oxide (D_2O, 99.9 atm%) was obtained from the Sigma-Aldrich Chemical Company (Castle Hill NSW, Australia). Formic acid (~98%, Fluka) was obtained from Sigma-Aldrich Chemical Company (Castle Hill NSW, Australia). Sodium hydroxide (NaOH, technical grade) was obtained from Ajax Chemicals (Seven Hills

NSW, Australia). Trifluoroacetic acid (TFA, spectrophotometric grade, 99+%) was obtained from Sigma-Aldrich Chemical Company (Castle Hill NSW, Australia). All samples were introduced into the mass spectrometers by flow injection analysis (FIA). The concentration of the infused samples ranged from 0.5–10 ng/μL (depending upon the type of experiment and instrument used), using a ratio of 3:1 acetonitrile: water with 0.05% formic acid. FIA was conducted at a rate of 3 μL/min. Deuterium-exchange experiments were conducted using D_2O: acetonitrile mixture of 1:3. Agilent LC/MSD XCT ion trap mass spectrometer (Agilent Technologies) was used with an electrospray ionisation source operating in positive ion mode. The following conditions were applied to the instrument: mass range mode, standard enhanced (a resolution setting where full width half-height maximum is 0.35); high voltage, 4000 V; nebulizing gas pressure, 15 psi; drying gas flow, 7 L/min; drying gas temperature, 325 ºC; maximum accumulation time, 200 ms; ion charge control (an automated maximum trap loading control), 10^5 ions; averaged spectra, 5; all other lens were automatically optimized for the maximum transfer of ions using the Smart Parameter Setting (a component specific automated ramped fragmentation control). The following conditions were used for CID; helium pressure (inside the ion trap), 1.2 x 10^{-5} bar; and the fragmentation amplitude, 0.65 – 0.85. Accurate mass measurements were performed using a Bruker Apex II Fourier Transform Mass Spectrometer (FTMS) with an Analytical ESI source attached operated in positive ion mode (Bruker Daltonics). The following conditions were applied to the instrument for this study; nebulizing pressure, 35 psi; drying gas, 4 L/min; source temperature, 110ºC; cylinder voltage, -2188 V; capillary voltage, -3910 V; end plate voltage, -3480 V; data set size, 128 K; and accumulation time, 1 s. The instrument was calibrated using a 1 mM sodium hydroxide: 100 mM trifluoroacetic acid methanol solution, using the ions

produced at *m/z* 64.97739 (Na_2F, CID spectral calibration only), 158.96403 ($[TFA]Na_2$), 430.91365 ($[TFA]_2Na_3$) and 566.88846 ($[TFA]_3Na_4$). The mass spectral resolution at the lower end of the calibrated range was at least 45 000, with the range at the higher end being at least 16 000. In this paper, all masses are reported as nominal masses for the ease of discussion and where accurate masses were used to confirm the molecular formula; the formula is written next to the mass or structure.

Electronic Structure Calculations

Geometry optimizations were carried out with the B3LYP method[20,21] using the 6-311G(d,p) basis set within the GAUSSIAN03 suite of programs which specifies tight convergence criteria by default (SCF=TIGHT) for this approach.[22] All stationary points on the potential energy surface were characterized as either minima (no imaginary frequencies) or transition states (one imaginary frequency) by calculation of the frequencies using analytical gradient procedures. Frequency calculations provided zero-point energies, which were used – without empirical scaling factors – to correct the calculated electronic energy. The minima connected by a given transition state were confirmed by inspection of the animated imaginary frequency using the MOLDEN package[23] and by intrinsic reaction coordinate calculation.

RESULTS and DISCUSSION

Mass Spectrometry

The tandem mass spectrum of the $[VG+H]^+$ molecular ion (*m/z* 270) obtained on a quadrupole ion trap mass spectrometer is shown in Figure 2. The most abundant fragments ions are observed at *m/z* 100 and 197 and appear in a ratio of approximately 20:1. The elemental composition of these product ions, were established by accurate mass measurement (see Table 1), using an FTMS and were found to be $C_6H_{14}N$ (*m/z*

100.11226) and $C_6H_{14}O_3PS$ (*m/z* 197.03932), respectively.

Figure 2

Scheme 2.

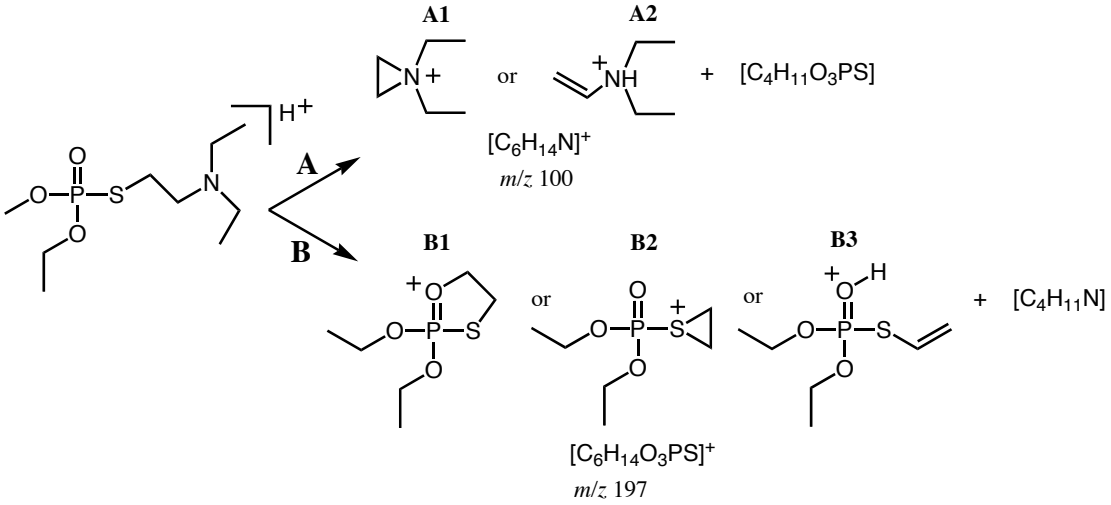

From the low and high resolution ESI-MS/MS data the ion at *m/z* 100 could correspond to the isomeric cations in Scheme 2. These ions have also been previously observed from protonated RVX.[17,19] The corresponding CID spectrum of the $[VG+D]^+$ ion, *m/z* 271, (Table 1) shows the base peak unchanged at *m/z* 100 (*N.B.*, CID spectra of both $[VG+H]^+$ and $[VG+D]^+$ show the ^{13}C-isotope peaks at *m/z* 101 with approximately equal abundance) which supports the structural assignment of the *N,N*-diethyl aziridinium cation (Scheme 2 A1) as a protonated amine ion (Scheme 2 A2) would be expected to at least partially incorporate the isotopic label. The analogous observation was reported for the CID of the $[VX+D]^+$ ion.[17]

Due to the intrinsic low mass cut-off of the quadrupole ion trap, no ions are observed in Figure 2 below the base peak at *m/z* 100. The FTMS CID spectrum of $[VG+H]^+$ however, found fragment ions at *m/z* 72 which were shown to be $C_4H_{10}N$ (*m/z* 72.08103) by accurate mass measurement. This fragmentation is consistent with the loss of ethylene from the *m/z* 100 ion. Loss of both *N*-ethyl substituents as neutral ethylene would result in protonated aziridine at *m/z* 44 (Scheme 3) as observed in MS^3 spectrum of the *m/z* 100 ion (Table 1). The neutral loss of *N*-alkyl substituents as an alkene was previously observed from VX[17] as well as in the CID spectra of protonated *N,N*-dialkylaminoethanols.[24]

Scheme 3.

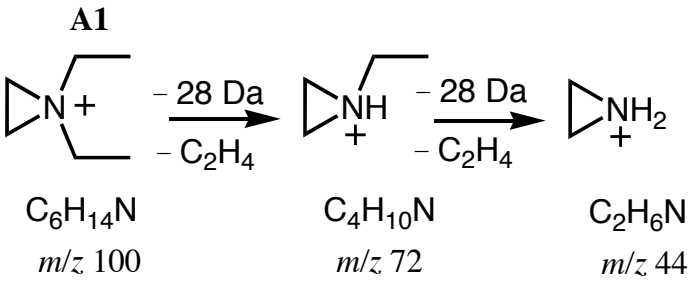

The fragment ion at *m/z* 197 in Figure 2 arises from the loss of neutral diethylamine from the $[VG+H]^+$ precursor. Three plausible molecular structures to account for this product ion are proposed in Scheme 2. The olefinic isomer B3 is protonated on oxygen which is inconsistent with deuterium labeling data, which shows no change to the *m/z* 197 ion upon fragmentation of $[VG+D]^+$ (Table 1) indicating that the deuterium is lost with the neutral diethylamine fragment. The two cyclic isomers (B1 and B2) are both consistent with the deuterium exchange data and are structurally related to the *m/z* 167 fragment ion formed upon dissociation of $[VX+H]^+$.[17] The MS^3 analysis of the *m/z* 197 fragment (Table 1) reveals two consecutive losses of ethylene (28 Da) to form ions at *m/z* 169.00814 ($C_4H_{10}O_3PS$) and *m/z* 140.97694 ($C_2H_6O_3PS$). These ions are also observed as minor secondary fragments in the CID spectrum of $[VG+H]^+$ (see inset expansion in Figure 2 and Table 1 for the high resolution data). This decomposition is most likely from the *O*-ethyl side chains as the loss of alkyl groups as neutral olefins by elimination from phosphorothiolate compounds is well documented in cases where the *O*-alkyl substituents are ethyl groups or larger (Scheme 4).[10,13,16,17,25] Low resolution CID of *m/z* 197 (Table 1) also reveals a fragment ion at *m/z* 109 resulting from the loss of 88 Da. This product ion is likely to arise from the loss of ethylene and thiirane in either a stepwise or concomitant process. The stepwise mechanism seems unlikely given that the direct loss of 60 Da, expected to be C_2H_4S, from *m/z* 197 is not observed. CID of *m/z* 197 (Table 1) also reveals a minor fragment ion at *m/z* 99 which is the result of stepwise loss of 70 Da to form a minor intermediate ion at *m/z* 127 followed by loss of ethylene (28 Da). In general, these MS^3 spectra do not clearly distinguish between the isomeric structures for *m/z* 197 proposed in Scheme 2. Although the observation of a fragmentation pathway involving the loss of neutral thiirane might indicate that the structure contains or rearranges to this motif (*cf.* Scheme 2B), in the absence of authentic

standards for comparisons no firm conclusions on the structure of the *m/z* 197 ion can be drawn from these data. In instances such as this computational data can often provide evidence based on the relative energetics of the various isomers and can also establish reasonable mechanisms by which they may be formed.

Scheme 4.

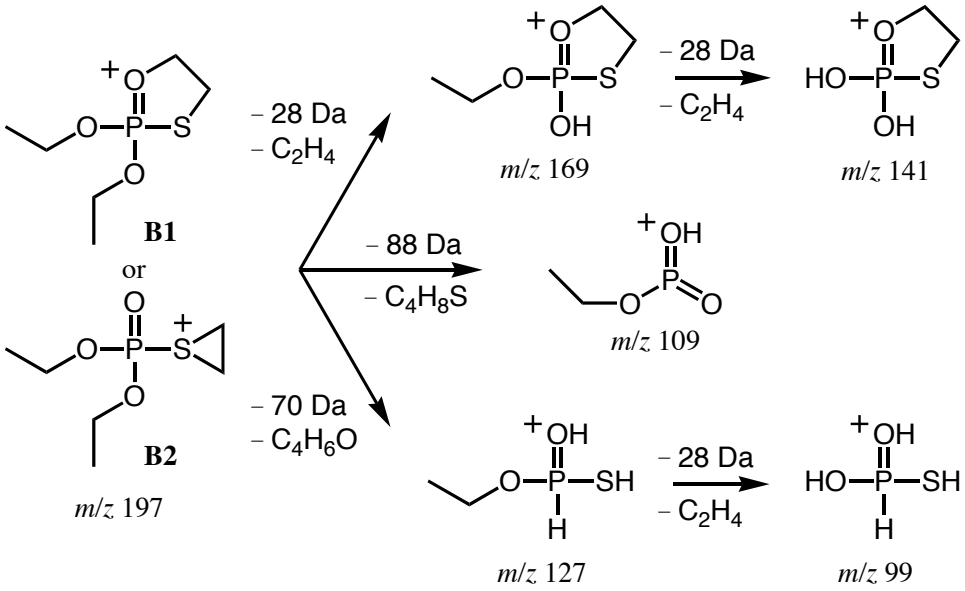

In addition to major *m/z* 197 and *m/z* 100 ions, a number of minor fragments are also observed from CID of $[VG+H]^+$, *m/z* 270 (Figure 2). The loss of ethylene (28 Da) from the *m/z* 270 precursor forms the *S*-[2-(diethylamino)ethyl]-*O*-ethyl hydrogen thiophosphate ion at *m/z* 242. MS^3 studies of the *m/z* 242 ion identify another loss of ethylene to produce *S*-[2-(diethylamino)ethyl] dihydrogen thiophosphate at *m/z* 214 (Table 1 and Scheme 5). The CID of $[VG+D]^+$ (Table 1) shows an increase in the *m/z* ratios for both of these fragment ions (*i.e.*, the corresponding ions appear at *m/z* 243 and *m/z* 215, respectively), indicating that the deuteron is retained by the charged fragment, which is consistent with an elimination process. The *m/z* 214 ion is not present at an intensity large enough to be observed in the CID spectrum of $[VG+H]^+$, which may suggest that the second loss of ethylene is slow compared to other fragmentation processes. It is interesting to note that the ethylene losses seen with $[VG+H]^+$ were not observed in the corresponding spectrum of VX although the analogous loss of isobutene is observed to a small extent for RVX.[17] This difference is most likely due to the availability of two *O*-alkyl substituents in VG compared to only one in each of the other homologues. The fragmentation of the *m/z* 242 ion in an MS^3

experiment (Table 1) produced an abundant ion at *m/z* 100 consistent with the diethyl aziridine structure formed directly from the protonated VG (Scheme 2). The observation of this secondary fragment strongly suggests that the loss of ethylene from the $[VG+H]^+$ precursor arises from the *O*-ethyl rather than the *N*-ethyl moieties. MS^3 of *m/z* 242 also reveals a loss of 108 Da to form the *m/z* 134 fragment ion. A plausible molecular formula for the loss of 108 Da is $C_2H_5O_3P$ which would suggest the formation of 2-(diethylamino)ethanethiol following proton transfer to sulphur (Scheme 5). This proposal is supported by the deuterium exchange studies (Table 1), which show the formation of *m/z* 135 from the deuterated precursor *m/z* 243. Finally, fragmentation of *m/z* 242 results in a product ion at *m/z* 196, which corresponds to a loss of ethanol (46 Da).

Scheme 5.

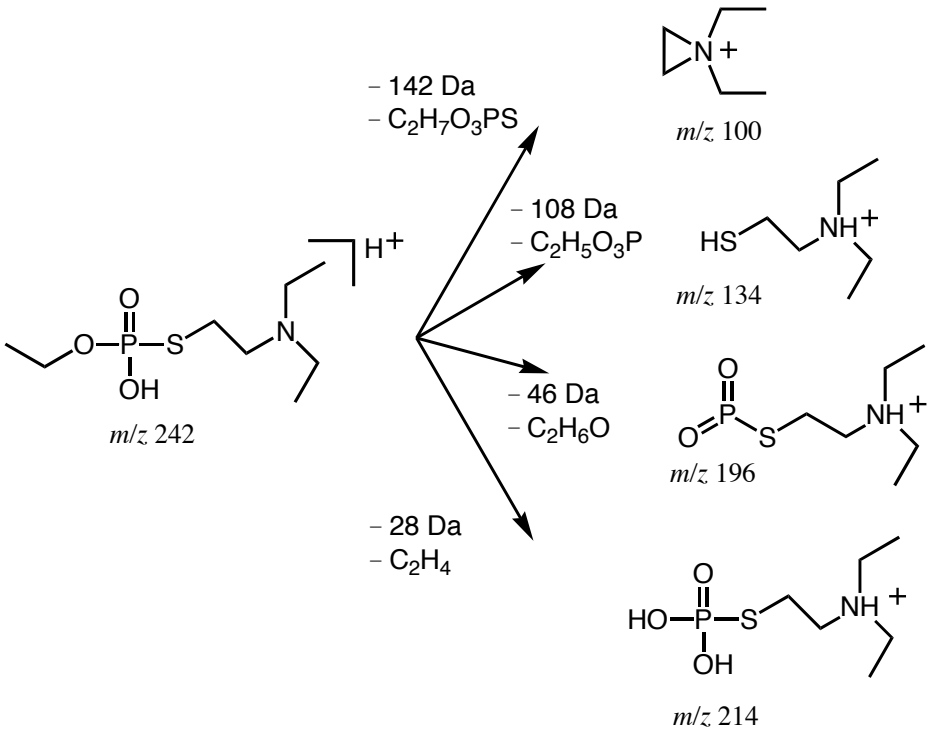

Electronic Structure Calculations

Given the molecular size and the number of conformational degrees of freedom in the VG molecule, electronic structure calculations were carried out on the simplified model system shown in Figure 3 where the ethyl substituents are represented by hydrogen atoms. The effects of this simplification on the structure and energetics of stationary points on the potential energy surface are included in the discussion below.

Figure 3.

Geometry optimization of the model VG structure at the B3LYP/6-311G(d,p) level resulted in the location of several local minima but the lowest energy conformation is shown in Figure 4(a). This minimum has a cyclic structure with a strong H-bonding interaction between nitrogen and one of the hydroxyl moieties on the phosphorous. Such stabilizing interactions are not possible in VG itself and thus the open chain local minimum shown in Figure 4(b) provides a better model structure for the target compound. This local minimum is 38 kJ mol^{-1} more energetic than the cyclic conformation. Protonation occurring during electrospray ionisation can potentially occur on nitrogen, oxygen or sulphur and structures for the respective isomers are shown in Figure 4(c), (d) and (e), respectively. The calculations reveal that protonation on nitrogen is favoured by about 75 kJ mol^{-1} over protonation on oxygen and by more than 150 kJ mol^{-1} over protonation on sulphur. These data suggest that during the relatively soft electrospray ionisation of VG, most of the analyte molecules will protonate initially on nitrogen and fragmentation processes may be preceded by proton transfer reactions. Comparison of the relative energies of the neutral (open chain) and the cation protonated on nitrogen provide a proton affinity of 980 kJ mol^{-1} for the model system. The proton affinity of VG is likely to be higher, however, as alkyl substitution of amines is known to significantly increase the stability of the ammonium cation and thus increase the proton affinity of the amine in the gas phase. For example, the gas phase proton affinity of ammonia is 853.6 kJ mol^{-1}compared with 952.4 kJ mol^{-1} for diethyl amine.[26]

Figure 4.

Figure 5.

Using the model system, reaction coordinates have been calculated for the two major fragmentation processes of the $[VG+H]^+$ cation. The relative energies of transition states, reaction intermediates and products are shown pictorially as a reaction coordinate diagram in Figure 5. The energies of all significant stationary points are given in Table 2. Figure 5 shows that while protonation on nitrogen is energetically

favoured, proton transfer to oxygen or even sulphur are relatively low energy processes compared to dissociative reaction channels. As a consequence unimolecular rearrangements and dissociations stemming from each of these minima need to be considered.

Let us first consider reaction channels resulting in formation of $C_2H_6N^+$ ions that are analogous to the diethylaziridine ion at *m/z* 100 observed as the base peak in the fragmentation of $[VG+H]^+$. The calculations reveal that, considered in isolation, protonated aziridine is 40 kJ mol^{-1} more energetic than protonated aminoethylene, however, reaction pathways resulting in formation of the latter have significantly higher activation energies. The transition state, TS1 (Figure 5), connects the model-VG, protonated on oxygen, with the protonated aziridine exit channel. The structure of TS1, shown in Figure 4f, is consistent with a nucleophilic substitution reaction with nitrogen-centred nucleophile attacking carbon and displacing the thiophosphate leaving group (Scheme 6a). The relative energy of this transition state, and thus the activation energy for the substitution reaction, is some 47 kJ mol^{-1} lower than that for the elimination reaction (Scheme 6b) from the nitrogen-protonated precursor via the transition state TS4 (Figure 4i). The thermodynamic favourability of the nucleophilic process predicted by calculation is consistent with the experimental assignment of the structure of *m/z* 100 exclusively to the *N,N*-diethyl aziridinium ion.

Scheme 6.

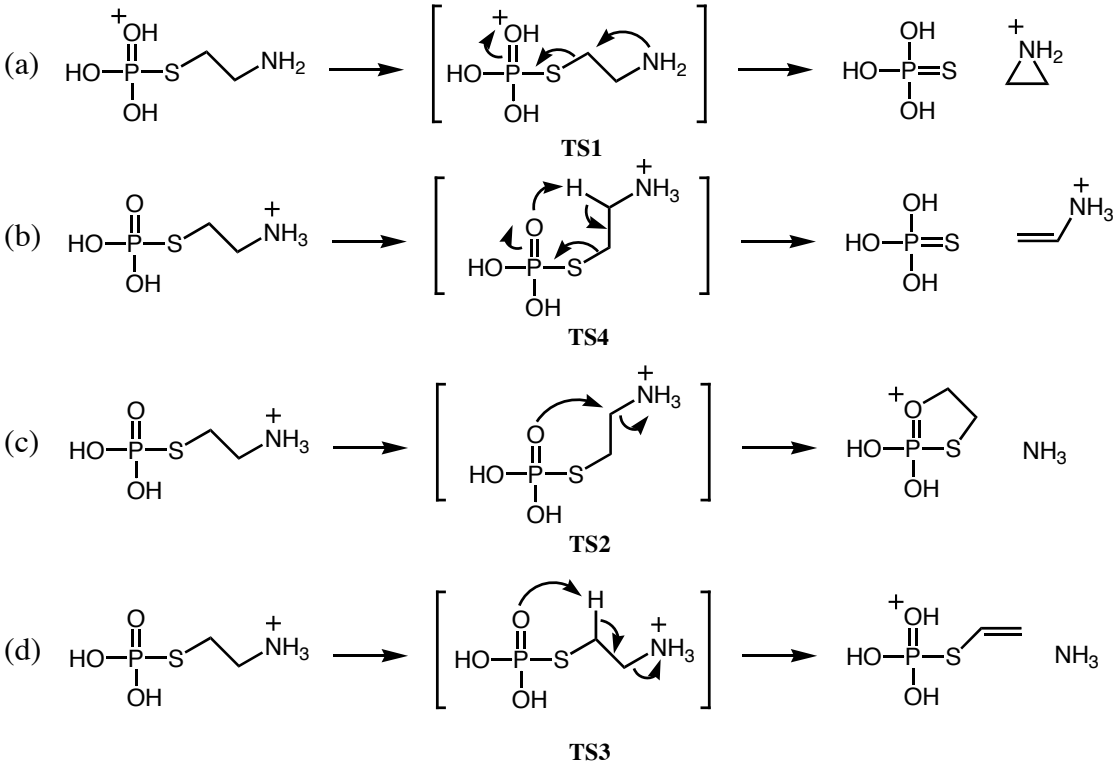

The calculations also compare the relative energy of $C_2H_6O_3PS^+$ ions by analogy to the range of isomers that could be responsible for the *m/z* 197 observed in the fragmentation of $[VG+H]^+$ (Scheme 2). The data show that the 5-membered ring (Figure 4k, analogous to B1 in Scheme 2) is the more stable than the olefinic isomer (Figure 4l, analogous to B3 in Scheme 2) by 30 kJ mol^{-1} while the thiirane structure is significantly higher in energy (Figure 4m, analogous to B2 in Scheme 2). The calculations show that the transition state for nucleophilic substitution is lower in energy than the comparable elimination process by almost 30 kJ mol^{-1} (Scheme 6c and d, respectively). As previously discussed, the deuterium labeling experiments exclude the olefinic isomer, B3, and thus the elimination mechanism (Scheme 6d). No transition state for the formation of the thiirane structure could be located, however given the relative energies of the fragmentation products (202.5 kJ mol^{-1}) this pathway does not represent an energetically competitive process. The combination of computational and experimental data, therefore, suggest that the ion observed at *m/z* 197 should be attributed to the structure labeled B1 in Scheme 2.

Lastly, it is significant to compare the computed energetics of the two major reaction pathways observed experimentally which produce ions at *m/z* 100 and 197. The respective barriers for these processes, namely TS1 and TS2, are within 5 kJ

mol^{-1} of each other with the aziridine forming reaction requiring slightly less activation energy. Interestingly, dissociation of the post-reactive complex to separated products requires and additional 43 kJ mol^{-1} giving an effective activation barrier to this reaction channel of 173 kJ mol^{-1}, which is greater than the 160 kJ mol^{-1} activation barrier to the minor *m/z* 197 ion forming channel. These computational data would thus predict that formation of *m/z* 197 should be favoured over formation of *m/z* 100: a prediction at odds with the experimentally observed abundances of these two ions (see Figure 2). This discrepancy is due to the failure of the model system used for these calculations to consider the effect of the *N*-ethyl substituents present in VG. While overall, the model system provides a good approximation for the chemistry of protonated VG, as previously discussed *N*-alkylation of amines increases the stability of nitrogen centred cations, which can have a significant impact when comparing these two product channels. This effect is simply corrected by re-calculating the relative energy of the two exit channels while including two ethyl groups on each nitrogen. These calculations show the *N,N*-diethyl aziridinium cation product channel is favoured *ca.* 10 kJ mol^{-1} over the competitive channel producing neutral diethyl amine (data provided in Table 2). Furthermore, by the Hammond postulate the lowering of the energy of the exit channel as a result of ethyl substitution is likely to result in a concomitant lowering of the energy of TS1 relative to TS2. Thus the computational result would predict a greater abundance of *m/z* 100 ions compared to *m/z* 197 ions as observed experimentally.

Table 2.

CONCLUSION

The fragmentation patterns of $[VG+H]^+$ have been investigated, the most abundant fragments in the tandem mass spectrum of protonated VG are observed at *m/z* 100 and 197. The *m/z* 197 fragment, has an elemental composition that could suggest a range of possible isomers. Hybrid density functional calculations strongly favour the structure shown as B1 in Scheme 2 based on the computation of relative energies of these structures and the activation energies for dissociation processes. The fragments observed for $[VG+H]^+$ are analogous to cleavages previously reported for homologous compounds including VX, RVX and *N,N*-dialkylaminoethanols and thus the calculated reaction coordinates in this study provide a detailed insight into the

unimolecular fragmentation behaviours of this class of molecules. The results from this study suggest that ESI-MS/MS may be useful for the to rapid identification of unknown organophosphorus CWAs.

ACKNOWLEDGEMENTS

SE acknowledges the following people who assisted with this research; Joe Moniodos from the School of Biomedical and Chemical Sciences University of Western Australia for preliminary molecular modelling work; Harry Rose, Veronica Borrett, Barry Lakeland, David Bourne, Justin Doward and Robert Mathews from the Human Performance and Protection Division of the Defence Science and Technology Organisation for providing comments to the manuscript. SJB and AR acknowledge the support of the Australian Research Council (DP0452849) and the Australian Partnership for Advanced Computing (ANU, Canberra) for a generous allocation of processor time through the Merit Allocation Scheme.

Table 1. Additional mass spectra obtained in this study.

Precursor ion (MS^n)	Product ions *m/z* (%abundance, elemental composition)[a]
$[VG+H]^+$ (MS^2)	270(5), 242(2), 197(3), 169(1), 141(1), 101 (8), 100(100)
$[VG+H]^+$ (MS^2), high resolution	270.12806(8, $C_{10}H_{25}NO_3PS$), 254.94345 (1), 242.09744(1, $C_8H_{21}NO_3PS$), 197.03932(1, $C_6H_{14}O_3PS$), 186.99466 (1), 169.00814(1, $C_4H_{10}O_3PS$), 140.97694(1, $C_2H_6O_3PS$), 100.11226(100, $C_6H_{14}N$), 72.08103(3, $C_4H_{10}N$).
$[VG+D]^+$ (MS^2)	271(4), 243(2), 197(4), 169(1), 141(1), 101(7), 100(100)
$[VG+H-C_4H_{11}O_3PS]^+$ (MS^3),	100(6), 72(100), 44(11)
$[VG+H-C_4H_{11}O_3PS]^+$ (MS^3), high resolution	100.11121(48, $C_6H_{14}N$), 72.08072(95, $C_4H_{10}N$), 44.04975(100, C_2H_6N)
$[VG+H-C_4H_{11}N]^+$ (MS^3)	197(15), 169(100), 141(53), 127(2), 109(6), 99(4)
$[VG+H-C_2H_4]^+$ (MS^3)	242(20), 214(9), 196(6), 169(2), 141(1), 134(49), 100(100), 74 (2), 72(2)
$[VG+D-C_2H_4]^+$ (MS^3)	243(30), 215(8), 197(4), 135(34), 100(100), 75(2), 72(2)

[a] Ion abundance is given as a percentage relative to the base peak in the spectrum.

Table 2. Optimized stationary points calculated for proposed fragmentation. Electronic energy, zero-point energy, relative energy and imaginary frequency calculated at B3LYP/6-311G(d,p) level of theory.

Structure	**Energy** (Hartrees)	**Zero-point correction** (Hartrees)	**Relative Energy** (kJ mol^{-1})
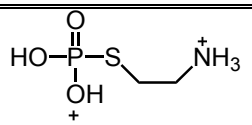	-1101.61720	0.13397	0
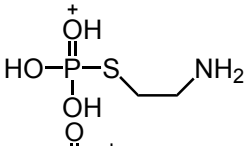	-1101.58914	0.13429	74.5
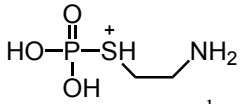	-1101.55315	0.12978	156.9
TS1 (-374 cm^{-1})	-1101.55334	0.12942	155.7
TS2(-438 cm^{-1})	-1101.55166	0.12967	160.7
TS3(-398 cm^{-1})	-1101.53890	0.12721	187.9
TS4(-583 cm^{-1})	-1101.53447	0.12836	202.5
TS5(-342 cm^{-1})	-1101.53127	0.12673	206.7
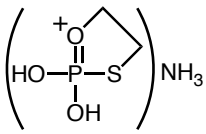	-1101.57841	0.12966	90.4
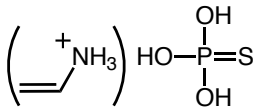	-1101.59436	0.13084	51.9

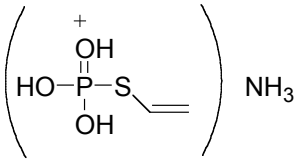	-1101.55729	0.12570	135.6
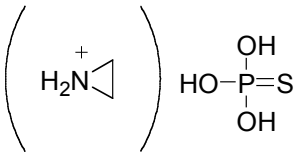	-1101.56790	0.13176	123.4
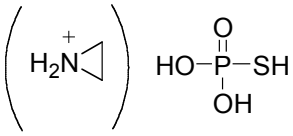	-1101.56956	0.12995	114.6
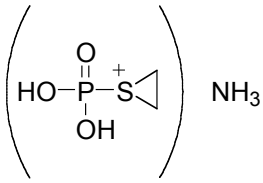	-1101.55381	0.12775	149.8
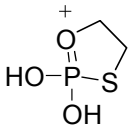	-1044.98262	0.09400	-
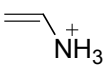	-134.332473	0.08325	-
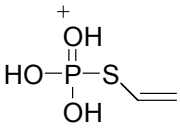	-1044.96541	0.08914	-
	-134.321873	0.08436	-
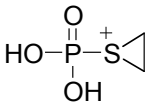	-1044.95570	0.09109	-
NH_3	-56.57603	0.03430	-
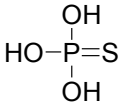	-967.22638	0.04642	-
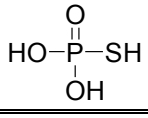	-967.21991	0.04362	-

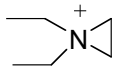	-291.63118	0.19691	-
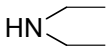	-213.85888	0.14882	-
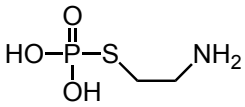 H-bonded conformer	-1101.22976	0.119699	980
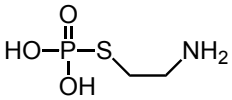 open chain conformer	-1101.24581	0.121318	941

FIGURES

Figure 1.

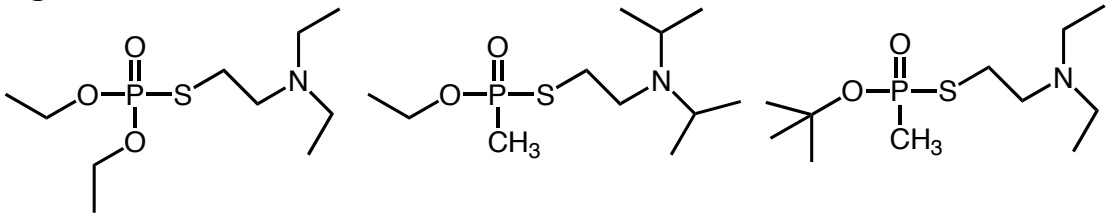

(a) VG (b) VX (c) RVX

Figure 2.

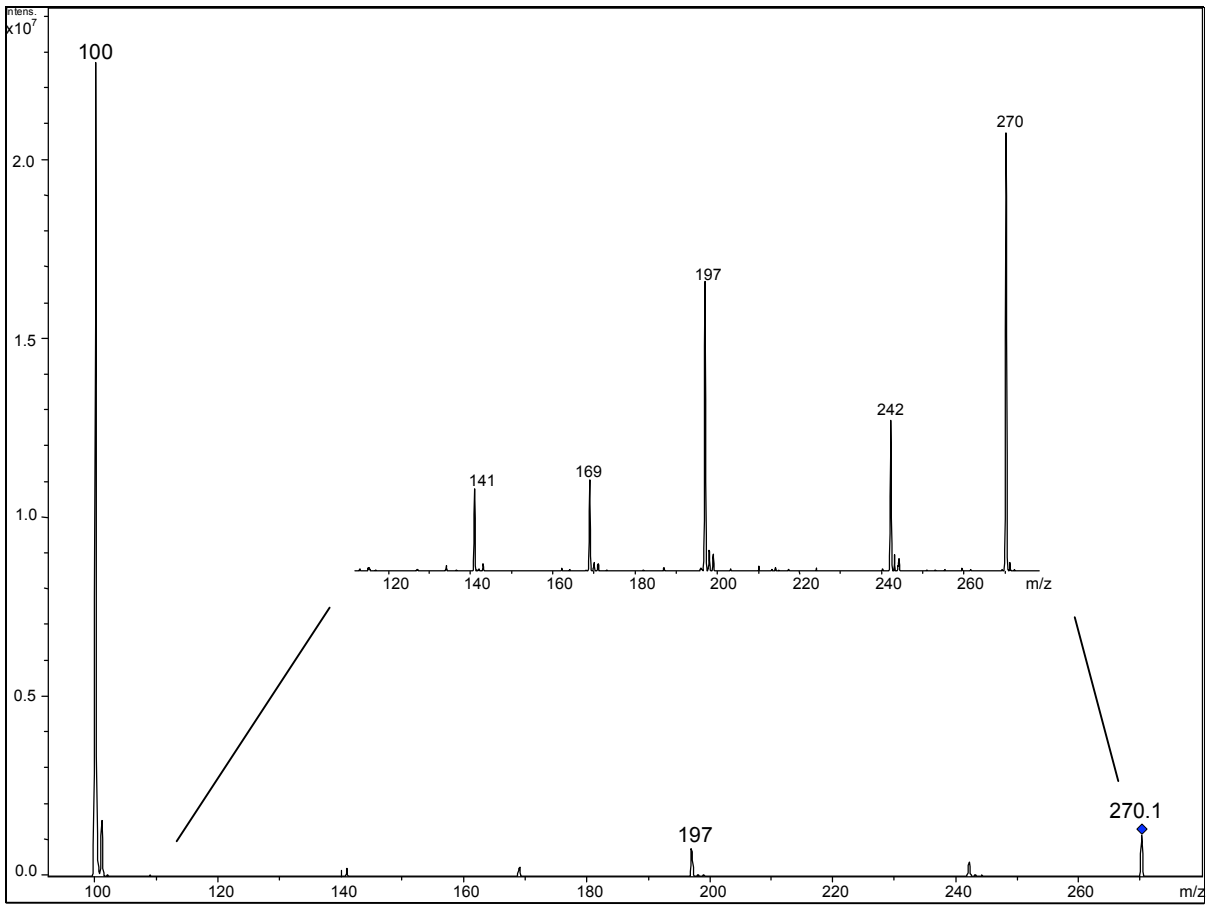
Intens.
x10^7
2.0
1.5
1.0
0.5
0.0
100
270
197
242
141
169
120
140
160
180
200
220
240
260
m/z
197
270.1
100
120
140
160
180
200
220
240
260
m/z

Figure 3.

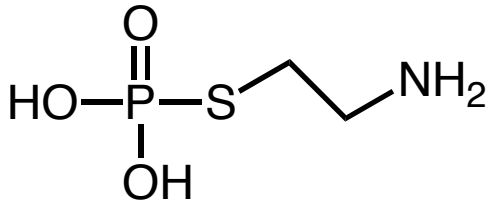

Figure 4.

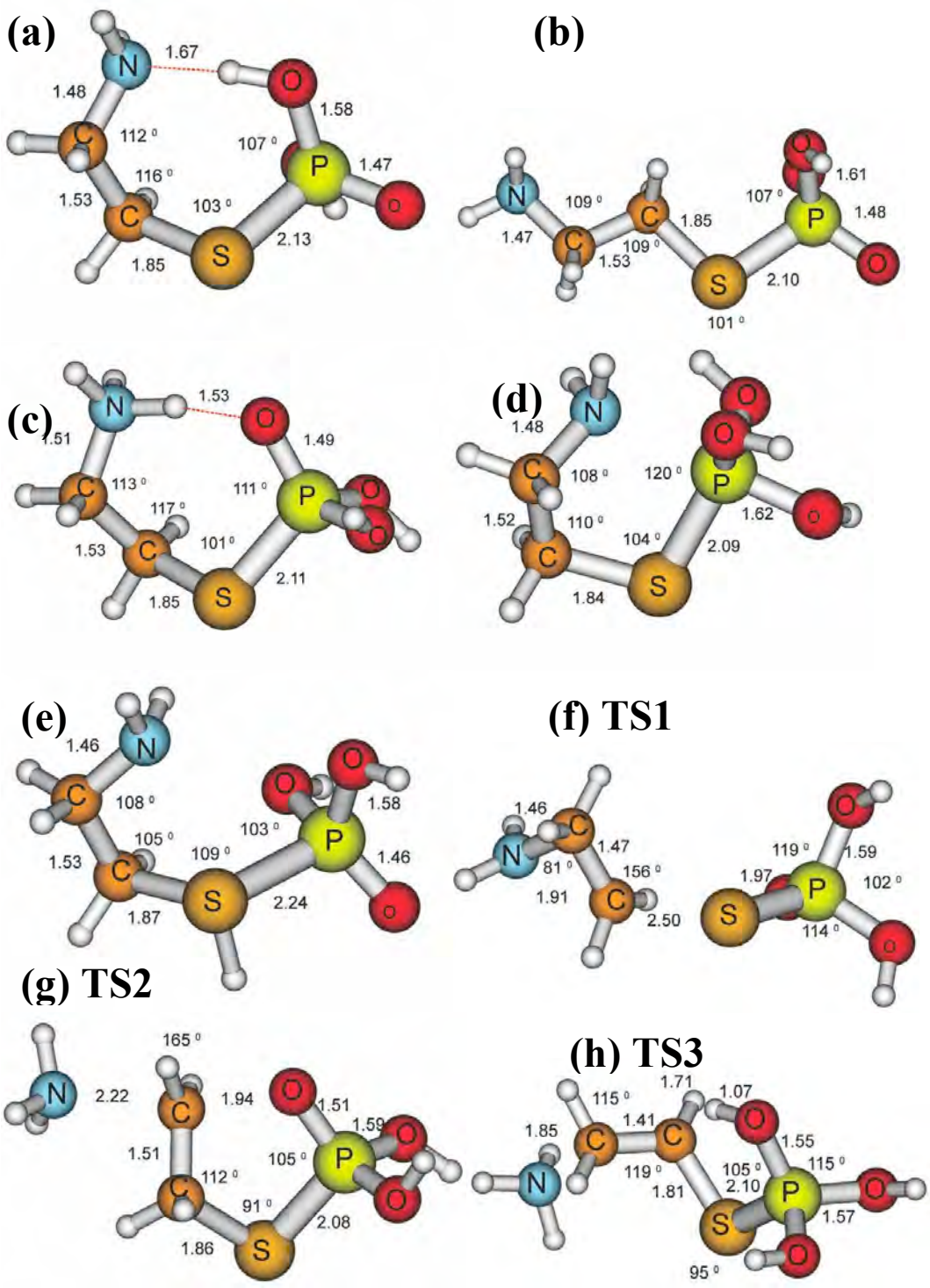

(i) TS4

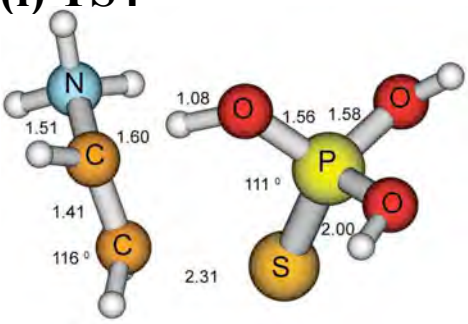

(j) TS5

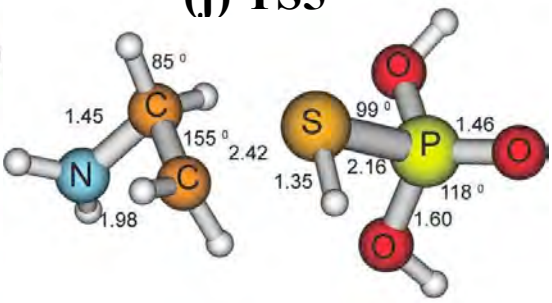

(k)

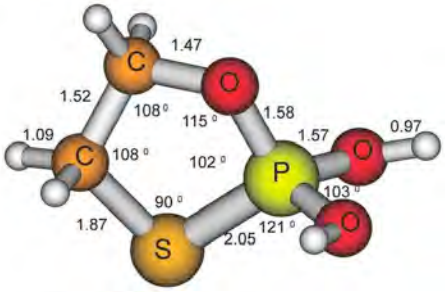

(l)

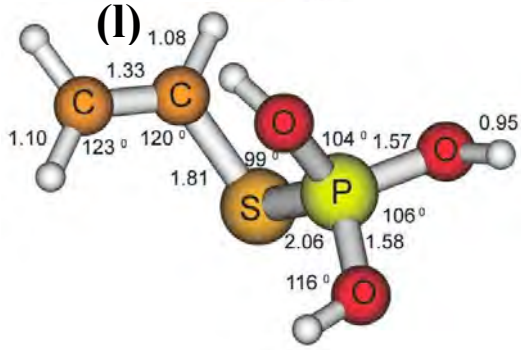

(m)

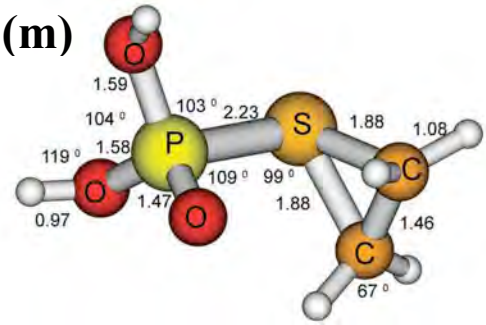

Figure5

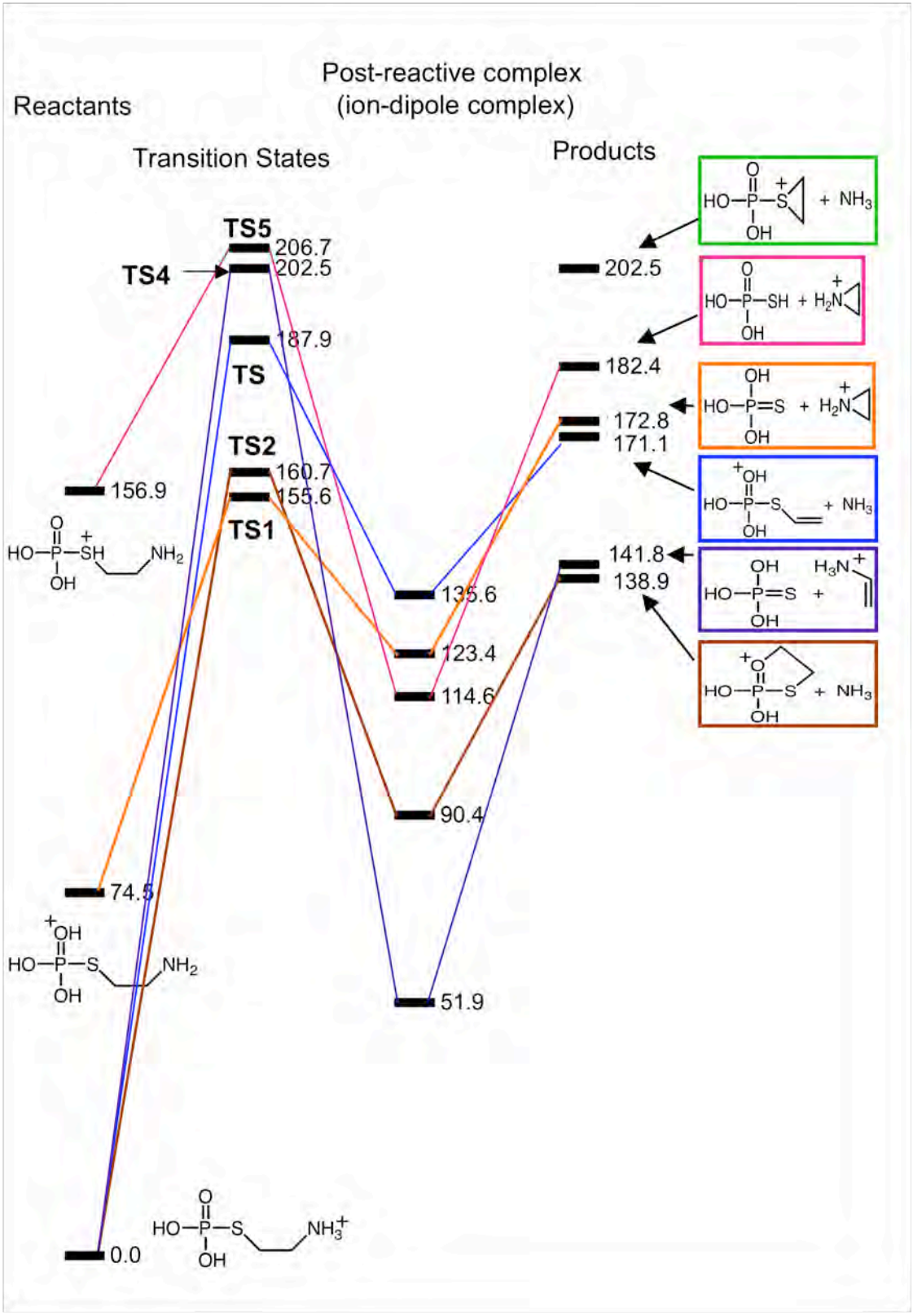
Reactants
Post-reactive complex
(ion-dipole complex)
Transition States
Products
TS5
206.7
TS4
202.5
187.9
TS
TS2
160.7
155.6
TS1
156.9
74.5
0.0
135.6
123.4
114.6
90.4
51.9
202.5
182.4
172.8
171.1
141.8
138.9
+ NH3
+ H2N
+ NH3
+ NH3

.

FIGURE CAPTIONS

Figure 1. The structures of (a) VG (Amiton), (b) VX and (c) RVX (Russian VX).

Figure 2. ESI-MS/MS mass spectrum of protonated VG. The spectrum was obtained using an Agilent LC/MSD XCT quadrupole ion trap mass spectrometer. The insert is an expansion of the less prominent ions between the *m/z* 120 and 270 and is magnified by a factor of 10.

Figure 3. The structure model VG used for the computational component of this study. Note that ethyl substituents in VG are represented by hydrogen atoms.

Figure 4. The structures derived from electronic structure calculations carried out at the B3LYP/6-311G(d,p) level for critical stationary points on the potential energy surface of model VG.

Figure 5. The potential energy surface of the protonated VG model system. All energies were calculated at the B3LYP/6-311G(d,p) level of theory and are given in units of kJ mol^{-1} and include unscaled zero-point energy corrections. The third column of minima represent post reaction ion-dipole complexes (structures not shown).

REFERENCES

1. *The Convention on the Prohibition of the Development, Production, Stockpiling and Use of Chemical Weapons and on their Destruction.* United Nations Document CD/1170: Geneva, August 1992.
2. Franke, S, *Manual of Military Chemistry. Chemistry of Chemical Warfare Agents (english tranlation)*. Deutsche Militarverlag: [East] Berlin, 1967; Vol. 1.
3. Ember, L. *Chem. Eng. News* 1989, 23.
4. Borrett, VT; Gan, TH; Lakeland, BR; Leslie, DR; Mathews, RJ; Mattsson, ER; Riddell, S; Tantaro, V. *J. Chromatogr. A* 2003; **1003**, 143.
5. Miettinen, J; Hirsjarvi, P; Pirila, L, *Chemical and Instrumental Verification of Organophosphorus Warfare Agents.* Ministry for Foreign Affairs of Finland: Helsinki, 1977; p 55.
6. Baum, G; Ward, FB. *Anal. Chem.* 1971; **43**, 947.
7. Bao, H; Yan, K; Liu, E. *Fenxi Huaxue* 1984; **12**, 723.
8. Yan, K; Wang, X; Huang, Y; Jia, Y. *Huanjing Huaxue* 1986; **5**, 15.
9. Borrett, VT; Colton, R; Traeger, JC. *Eur. Mass Spectrom.* 1995; **2**, 131.
10. D'Agostino, PA; Hancock, JR; Provost, LR. *J. Chomatogr. A* 1999; **840**, 289.
11. D'Agostino, PA; Hancock, JR; Chenier, C. *Eur. J. Mass Spectrom.* 2003; **9**, 609.
12. D'Agostino, PA; Hancock, JR; Provost, LR. *J. Chomatogr. A* 1999; **837**, 93.
13. Black, RM; Read, RW. *J. Chromatogr. A* 1998; **794**, 233.
14. Black, RM; Read, RW. *J. Chromatogr. A* 1997; **759**, 79.
15. Brickhouse, MD; Creasy, WR; Williams, BR; Morrissey, JR; O'Connor, R; Durst, HD. *J. Chromatog. A.* 2000; **883**, 185.

16. Creasy, WR. *J. Am. Soc. Mass Spectrom.* 1999; **10**, 440.

17. Bell, A; Murrell, J; Timperley, C; Watts, P. *J. Am. Soc. Mass Spectrom.* 2001; **12**, 902.

18. Groenewold, GS; Appelhans, AD; Gresham, GL; Olson, JE; Jeffery, M; Wright, JB. *Anal. Chem.* 1999; **71**, 2318.

19. Groenewold, GS; Appelhans, AD; Gresham, GL; Olson, JE; Jeffery, M; Weibel, M. *J. Am. Soc. Mass Spectrom.* 2000; **11**, 69.

20. Becke, AD. *J. Chem. Phys.* 1993; **98**, 1372.

21. Lee, CT; Yang, WT; Parr, RG. *Phys. Rev. B* 1988; **37**, 785.

22. Frisch, MJ; Trucks, GW; Schlegel, HB; Scuseria, GE; Robb, M; Cheeseman, JR; Montgomery Jr., JA; Vreven, T; Kudin, KN; Burant, JC; Millam, JM; Iyengar, SS; Tomasi, J; Barone, V; Mennucci, B; Cossi, M; Scalmani, G; Rega, N; Petersson, GA; Nakatsuji, H; Hada, M; Ehara, M; Toyota, K; Fukuda, R; Hasegawa, J; Ishida, M; Nakajima, T; Honda, Y; Kitao, O; Nakai, H; Klene, M; Li, X; Knox, JE; Hratchian, HP; Cross, JB; Bakken, V; Adamo, C; Jaramillo, J; Gomperts, R; Stratmann, RE; Yazyev, O; Austin, AJ; Cammi, R; Pomelli, C; Ochterski, JW; Ayala, PY; Morokuma, K; Voth, GA; Salvador, P; Dannenberg, JJ; Zakrzewski, VG; Dapprich, S; Daniels, AD; Strain, MC; Farkas, O; Malick, DK; Rabuck, AD; Raghavachari, K; Foresman, JB; Ortiz, JV; Cui, Q; Baboul, AG; Clifford, S; Cioslowski, J; Stefanov, BB; Liu, G; Liashenko, A; Piskorz, P; Komaromi, I; Martin, RL; Fox, DJ; Keith, T; Al-Laham, MA; Peng, C; Nanayakkara, A; Challacombe, M; Gill, PMW; Johnson, B; Chen, W; Wong, MW; Gonzalez, C; Pople, JA *Gaussian 03, Revision C.02.*, C.02; Gaussian Inc: Wallingford CT, 2004.

23. Schaftenaar, G; Noordik, JH. *J. Comput.-Aided Mol. Design* 2000; **14**, 123.

24. Reddy, TJ; Mirza, SP; Saradhi, UVRV; Rao, VA; Vairamani, M. *Rapid Commun. Mass Spec.* 2003; **17**, 746.

25. Bell, AJ; Despeyroux, D; Watts, P. *Int. J. Mass Spectrom. Ion Processes* 1997; **165/166**, 533.

26. Afeefy, HY; Liebman, JF; Stein, SE Neutral Thermochemical Data. In NIST Chemistry WebBook, NIST Standard Reference Database Number 69. http://webbook.nist.gov